Investigation of the Lithium-Fluorine-Hydrogen Tripropellant System

H. A. ARBIT,* S. D. CLAPP,† AND C. K. NAGAI*
Rocketdyne, Division of North American Rockwell Corporation, Canoga Park, Calif.

Attainment of the high performance potential of the $Li/F_2/H_2$ tripropellant combination requires complete Li-F_2 reaction and efficient expansion of the two-phase combustion products. This paper reports measured performance using gaseous H_2 and thrust chamber configurations designed to satisfy these requirements. Thermodynamic analyses showed that, at chamber equilibrium, the fluorine is nearly completely reacted with the lithium rather than with the hydrogen. Lithium injector design criteria derived from experimental studies of liquid metal atomization led to thrust chamber concepts which gave c^* efficiencies of 97–100%. Heat flux measurements showed that regenerative cooling with liquid H_2 would be feasible for a practical engine. Measured specific impulse efficiency obtained under simulated altitude test conditions was 95%, corresponding to actual vacuum specific impulse of 523 lb_f/lb_m/sec deliverable by a regeneratively cooled, 100:1 expansion ratio engine at chamber pressure of 1000 psia, F_2/Li mixture ratio of 2.74, and H_2 proportion equal to 25% of total propellant flowrate.

Nomenclature

c^*, L^*	=	characteristic exhaust velocity and characteristic chamber length, respectively
D	=	diameter of orifice
D_{30}	=	volume mean diameter
F, M	=	thrust and momentum, respectively
I_{sp}	=	specific impulse
MR	=	mixture ratio ($\dot{w}_{oxidizer}/\dot{w}_{fuel}$)
P_c, T_c	=	chamber pressure and chamber temperature, respectively
Re, We	=	Reynolds number and Weber number, respectively
$V, \Delta V$	=	velocity and relative gas-liquid velocity, respectively
$\dot{w}$	=	weight flow rate
X_p	=	penetration of liquid stream into gas jet
ϵ	=	expansion ratio
θ	=	angle between liquid stream and injector face
μ, ρ, σ	=	viscosity, density, and surface tension, respectively

Subscripts

G, L	=	gas and liquid, respectively
vac	=	vacuum

Introduction

THE performance potential of the $Li/F_2/H_2$ tripropellant combination is among the highest available from chemical propellants.[3] Theoretical vacuum specific impulse at P_c = 1000 psia, F_2/Li MR = 2.74 (stoichiometric), H_2 = 28%, and ϵ = 100 is 538 lb_f/lb_m/sec. Corresponding values for F_2/H_2 (P_c = 1000 psia, F_2/H_2 MR = 12) and O_2/H_2 (P_c = 1000 psia, O_2/H_2 MR = 5) are 492 and 473 lb_f/lb_m/sec, respectively. Except for a few low-thrust tests (not reported in the open literature), no systematic experimental investigation of the practical feasibility of $Li/F_2/H_2$ for rocket propulsion has been carried out. The primary objective of the present effort was to determine the extent to which the high performance potential of this combination can be realized in thrust chambers approaching practical configurations. The investigation included: 1) a thermodynamic-kinetic analysis of the $Li/F_2/H_2$ system, including extensive theoretical performance calculations; 2) establishment of criteria for the achievement of high c^* efficiency, including experimental studies of liquid metal atomization and the development of appropriate tripropellant injection techniques; and 3) measurement of c^* efficiency, thrust chamber heat flux characteristics, and specific impulse in a 60:1 expansion ratio thrust chamber under simulated altitude conditions, using liquid lithium (LLi), liquid fluorine (LF_2), and gaseous hydrogen (GH_2). Nominal test conditions were P_c = 500–750 psia, F_2/Li MR = 2.2 to 5.0, H_2 = 15–40%, and F_{vac} = 2000 lb_f.

Chemical Characteristics of the $Li/F_2/H_2$ System

Concurrent reactions in a system consisting of all gaseous components were considered. This system would be at its lowest temperature (2500°R at the nominal test conditions) if the F_2 reacted only with H_2, leaving Li and excess H_2 to act as a heat sink. An activation energy of 17.4 kcal/mole was estimated for the F_2-H_2 reaction,[4,5] which apparently proceeds by an energy chain mechanism.[6,7] Extrapolation of available F_2-H_2 kinetic data[4] to 2500°R gave a predicted half-life of about 2 μsec; hence, the F_2-H_2 reaction reaches completion before significant vaporization of Li occurs, so that gaseous Li evaporating from the parent droplets reacts with HF. For the Li-HF reaction, the activation energy and the preexponential factor in the rate equation were estimated[8] as 11.2 kcal/mole and 10^8 $T^{\frac{1}{2}}$, respectively. At 2500°R, 500 psia, and 20 mole % HF, the predicted half-life of a Li atom is 0.2 μsec. Although the HF concentration decreases as the reaction nears completion and a number of half-lives are required to approach complete Li combustion, the Li-HF

Received May 4, 1970; revision received June 15, 1970. Portions of this paper were presented as Paper 68-618 at the AIAA 4th Propulsion Joint Specialist Conference, Cleveland, Ohio, June 12, 1968, and at the ICRPG Eleventh Liquid Propulsion Symposium, Miami Beach, Fla., September 18, 1969. This work was carried out under NASA Lewis Research Center Contracts NAS3-7954 (J. W. Gregory, Project Manager), and NAS3-11230 (S. M. Cohen, Project Manager). The material presented herein was condensed from the final reports prepared under these contracts.[1,2] The contributions of A. E. Axworthy, L. W. Carlson, R. A. Dickerson, G. A. Hosack, and K. W. Tate, all of the Rocketdyne Research Division, to the conduct of this study, are acknowledged with thanks.

* Member of the Technical Staff, Exploratory Engineering Section, Research Division. Member AIAA.

† Program Manager, Advanced Propulsion Technology, Research Division. Member AIAA.

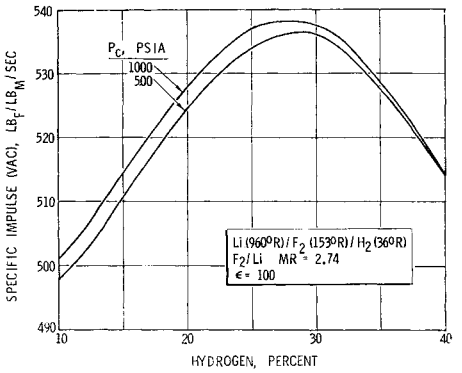

Fig. 1 Theoretical vacuum I_{sp} of the LLi/LF_2/LH_2 tripropellant combination vs H_2 percentage.

reaction is virtually complete in <10 μsec even under the most adverse conditions. The kinetics of the Li-F_2 reaction have not been studied. Virtually no activation energy would be predicted, since a relatively weak bond is being broken and the reaction is highly exothermic.[9] On this basis, and with the same pre-exponential factor as for Li-HF (which assumes that about one collision in 100 leads to chemical reaction), the predicted Li atom half-life is only 0.006 μsec at 2500°R. Thus, if an appreciable amount of Li should vaporize before HF formation is complete, the Li may inhibit further F_2-H_2 reaction by interruption of the chain mechanism. Under these conditions, Li vapor would react nearly instantaneously with F_2.

The combustion chamber equilibrium condition is that the F_2 is nearly completely reacted with the Li rather than with the H_2; i.e., the H_2 is essentially the rocket engine working fluid, as desired. Further, the chemical reactions in the tripropellant system proceed very much more rapidly than the physical processes of mixing and Li vaporization, so that the latter are the controlling factors in the attainment of complete Li combustion. As with more common propellant combinations, reaction kinetics do not significantly affect the combustion efficiency of the Li/F_2/H_2 system.

Theoretical performance calculations were made for ranges of parameters.[1] Typical results are presented in Figs. 1–3, which show, respectively, the variations of vacuum I_{sp} (shifting equilibrium) with H_2 proportion, F_2/Li mixture ratio, and expansion ratio for LLi/LF_2/LH_2. Maximum I_{sp} occurs at the stoichiometric F_2/Li mixture ratio and approximately 28% hydrogen. Substitution of solid Li (at 36°R) for liquid Li (at 960°R) decreases theoretical vacuum I_{sp} by approximately 4%, corresponding to the lower injection enthalpy. Theoretical, shifting equilibrium c^* and T_c (Fig. 4) also peak at the stoichiometric F_2/Li mixture ratio. Two-phase flow, arising from condensation of LiF, may be an important factor in the Li/F_2/H_2 combustion/expansion processes. The theoretical mass fraction of condensed material in the combustion products is a function of H_2 proportion, F_2/Li mixture ratio, and axial location (Figs. 5 and 6).

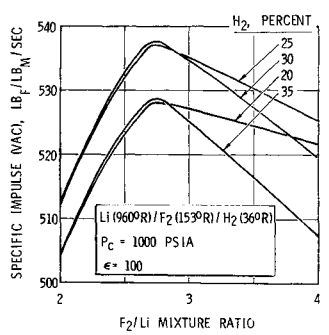

Fig. 2 Theoretical vacuum I_{sp} of the LLi/LF_2/LH_2 tripropellant combination vs F_2/Li mixture ratio.

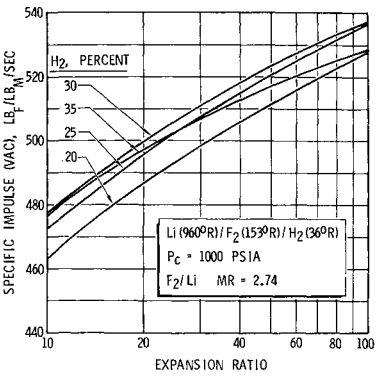

Fig. 3 Theoretical vacuum I_{sp} of the LLi/LF_2/LH_2 tripropellant combination vs expansion ratio.

Injection Methods

Lithium Droplet Combustion

The combustion of LLi drops is assumed to be a vaporization rate-limited process, complicated by the initial formation of LiF on the droplet surface.[10] A theoretical mechanism for the combustion of Li in an F_2 (or HF) atmosphere suggests that when the droplets are small, F_2 (or HF) diffuses through the thin, porous, surface layer of LiF. As the droplet temperature increases, the vapor pressures of the Li and LiF increase. The latter, which is exposed to the gas phase, is gradually vaporized and is also physically dislodged by the Li vaporizing from the droplet. The burning rate of the droplet then reaches a quasi-steady state in which it burns in a diffusion flame. For any initial droplet size, a constant fraction of its mass must be converted to LiF to heat the droplet to a given temperature, so that the nominal thickness of the LiF layer when the droplet reaches the Li boiling point is directly proportional to the initial droplet diameter. Consequently, the LiF layer on a large Li drop is relatively thick, which tends to slow the F_2 (or HF) diffusion and to inhibit the exothermic Li-F_2 (or Li-HF) reaction. For rapid and complete combustion, therefore, the Li atomization process must produce droplets which are small enough to burn by the "small droplet" mechanism.

A one-dimensional, vaporization rate-limited, steady-state combustion model[11] was used to calculate the effects of various parameters on c^* efficiency. This model considers the interrelated processes of droplet vaporization under forced convection, droplet drag and acceleration, and the flow dynamics of the combustion gases. Computations were made to define the fraction of Li vaporized and burned, and hence the combustion efficiency, as a function of mean droplet diameter, L^*, contraction ratio, and hydrogen proportion. Figure 7 shows typical results for computed c^* efficiency as a function of mean Li droplet diameter and L^* for LLi burning in gaseous F_2 in the absence of H_2. The sensitivity of combustion efficiency to lithium droplet size is apparent.

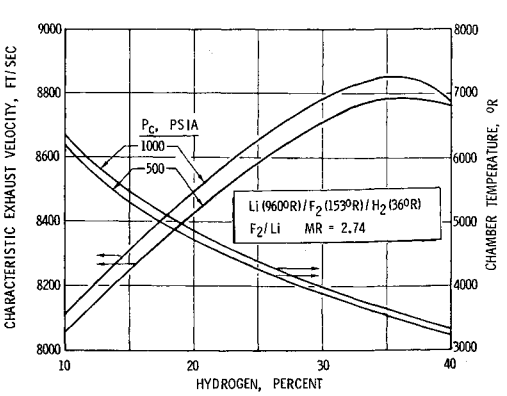

Fig. 4 Theoretical c^* and T_c of the LLi/LF_2/LH_2 tripropellant combination vs hydrogen percentage.

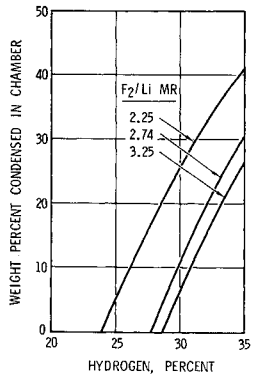

Fig. 5 Weight percent of condensed material (liquid LiF) in combustion chamber vs H_2 percentage (P_c = 750 psia).

Liquid Metal Atomization and Distribution

Atomization of LLi is relatively difficult because of its high surface tension (395 dynes/cm) compared to that of conventional liquid propellants (~25 dynes/cm). An extremely efficient atomization method is therefore required to produce the small Li droplets necessary for high combustion efficiency. A proven technique is the aerodynamic atomization of a liquid stream by a high-velocity gas jet. Specific design criteria and a propellant distribution factor for this mode of gas/liquid injection were established by experimental correlations defining the degrees of liquid atomization and of distribution uniformity as functions of pertinent parameters. Droplet sizes resulting from the aerodynamic atomization of liquid Cerrosafe‡ by gaseous N_2 in a triplet element (two liquid metal streams impinging within a central gas jet) were measured. Liquid injection velocity was 35–60 fps, gas injection velocity was 500–1100 fps, and liquid-to-gas mass flowrate ratio was 0.8–4.0. The spray produced by the element was directed into a collection vessel, the bottom of which was covered with water, and the solidified Cerrosafe droplets were sampled for photomicrographic size measurements. The observed volume mean droplet diameters were adequately expressed by the following modification of the Wolfe-Andersen equation[12]:

$$D_{30} = \phi[136\mu_L\sigma_L^{3/2}D_L^{1/2}/\rho_L^{1/2}\rho_G^2(\Delta V)^4]^{1/3} \quad (1)$$

where

$$\phi = \{3(\dot{w}_L/\dot{w}_G)/1 - [1 + (\dot{w}_L/\dot{w}_G)]^{-3}\}^{1/3} \quad (2)$$

The factor ϕ accounts for gas velocity decrease resulting from momentum exchange with the atomized liquid and therefore represents the increase in droplet size due to the finite ratio of gas to liquid flowrate. Equation (1) may be written as the ratio of volume mean droplet diameter to liquid

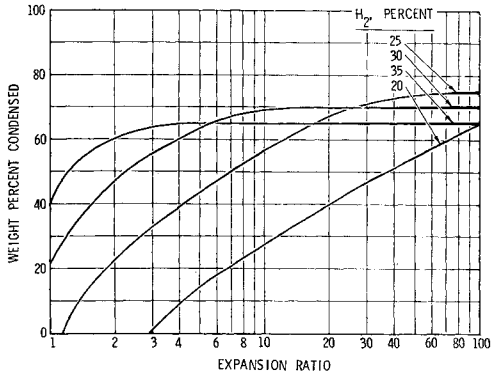

Fig. 6 Weight percent of condensed material in divergent nozzle vs expansion ratio (P_c = 750 psia). Thin lines represent liquid LiF; heavy lines, solid LiF.

‡ A low-melting, proprietary, bismuth-lead alloy (Cerro Sales Corp., New York) with surface tension of 400 dynes/cm.

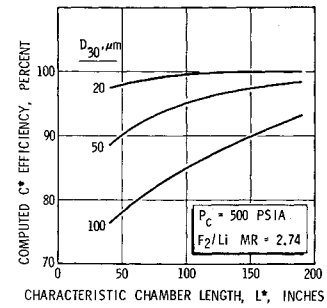

Fig. 7 Computed c* efficiency vs L^* for indicated initial Li droplet diameters.

stream diameter in terms of the liquid Reynolds number and the Weber number:

$$D_{30}/D_L = (5.14\phi/Re_L^{1/3}We^{1/2})(\rho_L/\rho_G)^{1/6} \quad (3)$$

A similar correlation has been obtained[13] from experiments in which the liquid/gas mass flowrate ratio was very small and the factor ϕ, therefore, was very nearly unity. Results of the present experiments also confirmed that the following conditional parameter[14] must be met to obtain the aerodynamic atomization to which Eq. (1) would be applicable:

$$We/(Re_G)^{1/2} \geq 1.0 \quad (4)$$

For maximum uniformity of propellant distribution, the atomized liquid should be dispersed across the gas jet diameter. Hence, the extent to which the liquid stream penetrates the gas jet is an important design factor for gas-liquid injectors. A photographic study was made of the penetration of gas jets by liquid streams in a triplet element. Nitrogen was used as gas simulant (jet diameters of 0.12–1.50 in.

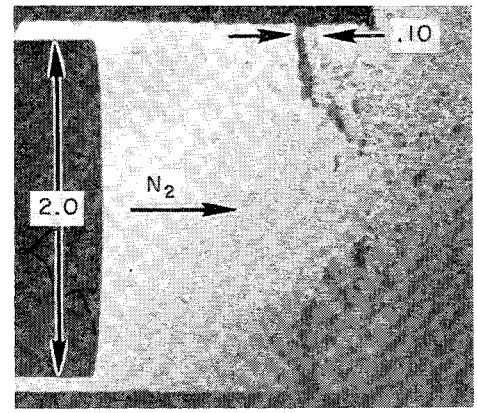

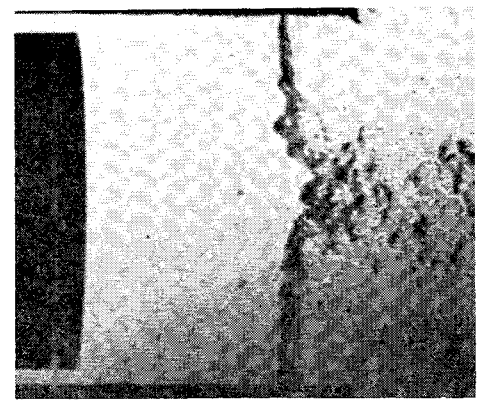

Fig. 8 Schlieren photographs showing (top) incomplete and (bottom) complete penetration of two 0.10-in.-diam He jets into a 2.0-in.-diam N_2 jet. [top) V_{He} = 650 fps, V_{N2} = 155 fps; bottom) V_{He} = 1300 fps, V_{N_2} = 155 fps.]

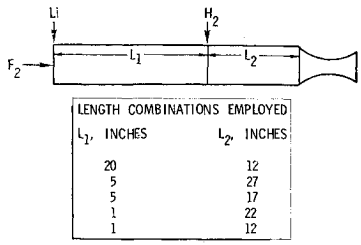

Fig. 9 Thrust chamber configurations used with the oxidizer-rich gas generator injection method (dimensions in inches). Chamber diameter is 5 in. in all cases.

and injection velocities of 400–1100 fps) and water or Cerrosafe was the liquid simulant (orifice diameters of 0.04 and 0.06 in. and injection velocities of 20–100 fps). On the basis of this study, the following empirical correlation was established for the ratio of penetration distance to liquid stream diameter:

$$X_P/D_L = [2.5(V_L \cos\theta)/V_G](\rho_L/\rho_G)^{1/2} \quad (5)$$

where $V_L \cos\theta$ is the liquid stream velocity component perpendicular to the gas jet. The penetration distance may also be expressed as a fraction of the gas jet injection diameter, in terms of the liquid/gas momentum ratio

$$X_P/D_G = (2.5 \cos\theta)(M_L/M_G)^{1/2} \quad (6)$$

Tripropellant Injection Methods

Two injection concepts were developed, both of which employed gas generators to produce the gas required for aerodynamic atomization of the *L*Li. The first method, representing optimum conditions for Li combustion (Li burning in an F_2 atmosphere at about 9800°R), used an oxidizer-rich gas generator in which the LF_2 was reacted with a very small fraction of the GH_2 (MR = 500) to produce vitiated GF_2 at 1000°R. This gas was injected with the Li into the main combustion chamber, and the bulk of the H_2 was injected at a downstream point. The second injection method represented the least favorable Li combustion conditions (Li burning in an HF atmosphere, in the presence of excess H_2, at ~4400°R). The atomizing gas (a mixture of HF and H_2) was produced in a fuel-rich gas generator in which the LF_2 was reacted with all of the GH_2 (MR ~2). Both the oxidizer-rich[1] and fuel-rich[2] LF_2/GH_2 gas generators were designed by standard procedures and gave c^* efficiencies of 96–100% when tested alone.

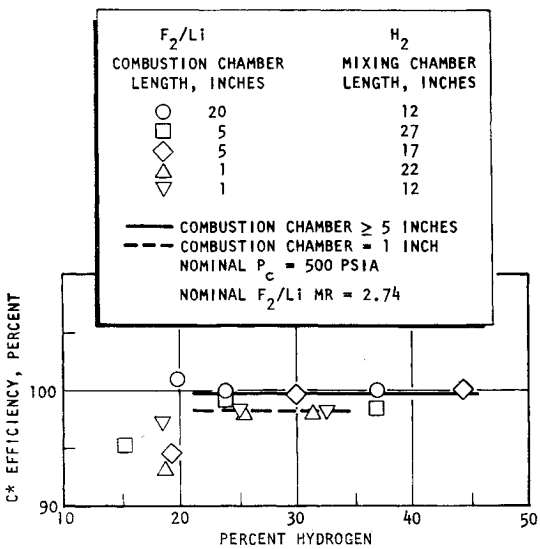

Fig. 10 Corrected c^* efficiencies vs percentage H_2 for the oxidizer-rich gas generator injection method at indicated test conditions.

Thrust Chamber Components and Lithium Facility

The Li/gas injector design which was used with the oxidizer-rich gas generator consisted of an 8-element doublet pattern (one Li stream injected into each gas jet). With the fuel-rich gas generator, a biplanar injector design was employed, wherein the single Li stream/single gas jet doublet was augmented by the impingement of four additional gas jets into the reacting central stream, downstream of the Li/gas impingement point. The auxiliary gas orifices were necessary because of the large quantity of gas produced in the fuel-rich gas generator. The eight Li injection orifices in both designs were individually fed through stainless steel or tantalum tubes (preferably the latter) joined to a heated external manifold. The Li/gas injectors consisted of ATJ graphite cores within stainless steel shells.

Injection velocities and orifice sizes were derived from Eqs. (1) and (5). Nominal volume mean Li droplet diameters and percentage penetration of the gas jet by the Li stream were, respectively, 11 μm and 80% with the oxidizer-rich gas and 6 μm and 80% with the fuel-rich gas.

When the oxidizer-rich gas generator was used, the bulk of the H_2 was injected into the combustion chamber downstream of the Li/gas injector. To obtain maximum uniformity of distribution across the chamber cross section, the H_2 was injected through 64 transversely-directed orifices arranged so that each one directly opposed another across the chamber. In effect, the impingement point of each pair became an H_2 injection point from which diffusion and turbulent mixing could begin. Design criteria were obtained empirically from Schlieren photographs (e.g., Fig. 8) of the penetration of high-velocity He jets into a low-velocity N_2 stream.

The uncooled combustion chambers consisted of 1.5-in.-thick ATJ graphite liners within carbon steel shells. The water-cooled combustion chamber consisted essentially of a copper liner within a stainless steel shell. Axial coolant passages were machined around the outer circumference of the liner.

Conical contour nozzles were used, with 15° convergence and divergence angles. The uncooled, low-expansion ratio nozzles consisted of ATJ liners within carbon steel shells. The water-cooled nozzle section (to ϵ = 3) consisted of a copper core with circumferential coolant passages machined around its outer surface, over which a layer of nickel was electroplated. Coolant entry and exit tubes were welded in the electroformed nickel plate. An uncooled extension was attached to the water-cooled nozzle for the altitude simulation firings. This skirt consisted of a thick-walled copper section from ϵ = 3 to ϵ = 10 and a mild steel section ($^3/_8$-in. wall) from ϵ = 10 to ϵ = 60.

A system for storing, heating, and delivering *L*Li to the test engine was designed and built, with austenitic stainless steel as structural material. Important system components were a 15-gal tank coded for 1300 psi at 600°F, a bellows-sealed main valve with integral valve seat, and a hot He purge gas subsystem. A burst diaphragm was installed immediately downstream of the main valve, to permit pre-test verification of valve functioning and to prevent entrainment of Li in the purge gas in the event of valve leakage. Lithium flowrate was measured with a magnetic flowmeter, and the Li system was heated by external electrical resistance heaters.

Characteristic Exhaust Velocity Efficiency

Oxidizer-Rich Gas Generator Injection Method

The uncooled thrust chamber configurations used in this test series represent successively smaller F_2/Li combustion chambers and H_2 mixing sections (Fig. 9). The final two configurations, with H_2 injection just 1 in. from the Li in-

jector, approximate the injection of all three propellants at the same axial location. Measured c^* efficiencies (corrected for heat loss to chamber, throat shrinkage, and throat discharge coefficient) are plotted in Fig. 10. At H_2 proportions below 20%, penetration of the H_2 jets into the combustion chamber is inadequate, and the resulting nonuniform distribution is reflected in erratically low c^* efficiencies. Above 20% H_2, the data fall into two groups: those from F_2/Li combustion chamber lengths ≥ 5 in. (corrected c^* efficiencies of ~99%) and those from the 1-in. chambers (corrected c^* efficiencies of ~98%). In the latter case, although the Li is still atomized by the GF_2, the presence of the H_2 in the injection region reduces the rate of diffusion of the F_2 to the Li droplets, lowers the temperature in the combustion region, and results in the reaction of Li with HF as well as with F_2. The fact that c^* efficiency is only very slightly reduced by injection of the H_2 within the F_2/Li combustion zone is evidence of the efficiency of the gas-augmented atomization process in producing extremely small Li droplets. It also leads to the prediction of comparable c^* efficiency levels if the Li were reacted with HF in the presence of H_2, as it is in the fuel-rich gas generator injection concept.

Fuel-Rich Gas Generator Injection Method

The test variables in the experimental firings using the fuel-rich gas generator were F_2/Li mixture ratio, proportion of H_2, and combustion chamber length. Corrected c^* efficiencies are shown in Fig. 11, in which the results at three H_2 percentage levels are plotted separately. At H_2 proportions below 30%, corrected c^* efficiency is essentially constant at ~97–98% over the experimental ranges of F_2/Li mixture ratio and H_2 percentage. At ~35% H_2, c^* efficiencies remain at this level with F_2/Li mixture ratios above stoichiometric, but decrease to ~93–95% below the stoichiometric F_2/Li mixture ratio. Indicated chamber length variations have no significant effect on c^* efficiency. The 97–98% c^* efficiencies are in agreement with the values predicted from the results of the Li/F_2/H_2 tests with the oxidizer-rich gas generator injection method. The data obtained with both injection methods also confirm the conclusion reached on the basis of the tripropellant reaction kinetics, namely, that the combustion chamber exit composition is the same whether the Li reacts with the F_2, with the HF, or with both.

The fuel-rich gas generator injection method is the simpler of the two Li/F_2/H_2 thrust chamber concepts, requiring one, instead of two, H_2 injectors and avoiding material problems associated with extremely high combustion chamber temperatures. It was therefore chosen for subsequent testing.

Heat Flux Characteristics

The thrust chamber used for measurement of Li/F_2/H_2 heat flux consisted of the fuel-rich gas generator, a 9-in.-long combustion chamber (formed by a 5-in., uncooled, upstream section and a 4-in., water-cooled segment adjacent to the nozzle), a water-cooled nozzle section to $\epsilon = 3$, and an uncooled nozzle skirt which extended to $\epsilon = 10$ in the sea-level tests and to $\epsilon = 60$ in the altitude simulation tests. Calorimetric methods were used to measure heat flux in the water-cooled portion of the thrust chamber, calibrated heat flux meters (thermocouples embedded in copper plugs) were employed in the nozzle between expansion ratios 3 and 10, and surface temperature measurements were used thereafter.

The heat flux measurements in the Li/F_2/H_2 firings were influenced by condensation and deposition of LiF (and some Li) on the walls of the water-cooled combustion chamber segment and in the entrance region of the water-cooled nozzle, and by the subsequent insulating effect of the coating. After a 6-sec firing, the thickness of the deposit was approximately 0.12 in. in the combustion chamber and at the

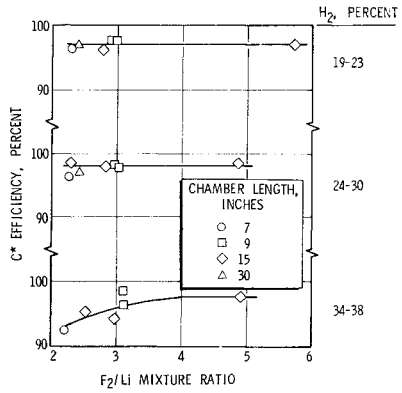

Fig. 11 Corrected c^* efficiencies vs F_2/Li mixture ratio for the fuel-rich gas generator injection method at indicated test conditions (nominal P_c = 750 psia).

start of nozzle convergence, beyond which it rapidly decreased to a few thousandths of an inch at the throat and in the expansion section. Estimated heat flux to the combustion chamber wall due to this condensation was approximately 5 Btu/in.^{2}/sec. The insulative effect of the coating was evidenced by a gradual decrease in heat flux as it built up.

Thrust chamber heat fluxes below and above the 30% H_2 level were qualitatively different, particularly in the throat region. This is shown in Fig. 12 (top) by Li/F_2/H_2 data at nominal levels of 20%, 25%, and 35% H_2. Results from an F_2/H_2 firing in the same engine are included for comparison. All data are normalized to 700 psia chamber pressure. The effect of wall condensation in the combustion chamber and start of convergence is reflected in the comparatively high heat flux in this region. In the nozzle, the curves for F_2/H_2 and for Li/F_2/H_2 with 20% and 25% H_2 are similar to each other and follow a normal pattern, with maximum heat flux immediately upstream of the geometric throat; heat flux at the 35% H_2 level, on the other hand, decreases in the throat region. The anomalous behavior at the highest proportion

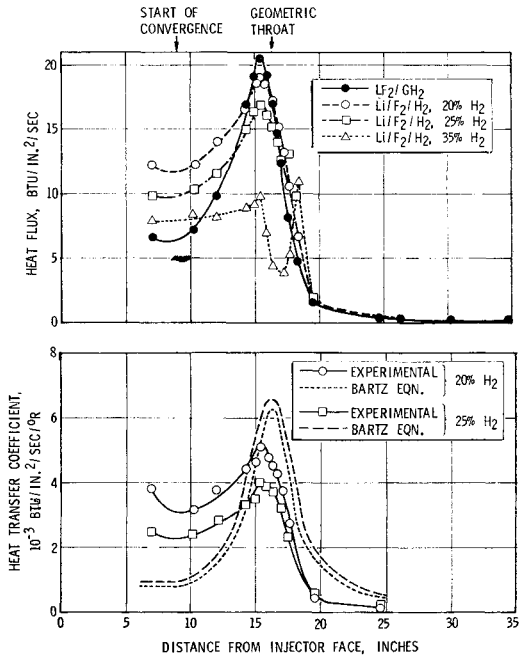

Fig. 12 Thrust chamber heat flux for F_2/H_2 (MR = 3) and for Li/F_2/H_2 at indicated proportions of hydrogen (all data normalized to 700 psia chamber pressure), and heat-transfer coefficients for Li/F_2/H_2 (P_c = 700 psia, F_2/Li MR = 2.74) compared with values calculated from the Bartz simplified equation.

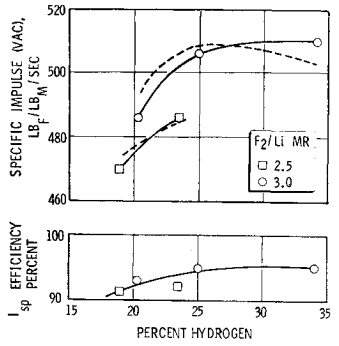

Fig. 13 Measured, uncorrected, vacuum I_{sp} and I_{sp} efficiency (solid curves) obtained in the altitude simulation firings (nominal P_c = 750 psia, ϵ = 60). Dashed curves represent vacuum I_{sp} deliverable by LLi (960°R)/LF_2 (153°R)/LH_2 (36°R) engine (ϵ = 60) cooled regeneratively with liquid hydrogen (P_c = 750 psia).

of hydrogen may be related to the fact that at F_2/Li mixture ratio of 2.74, condensation in the bulk flow begins downstream of the throat at the 20–25% H_2 levels, so that only gas-phase flow is present in the combustion chamber and throat region. With 35% H_2, however, a substantial portion of the product LiF is condensed in the combustion chamber, so that two-phase flow exists throughout the engine (Figs. 5 and 6). Experimental heat-transfer coefficients at 20% and 25% H_2 are compared with the corresponding Bartz equation[15] values in Fig. 12 (bottom). Again, the effects of wall condensation in the combustion chamber and entrance region of the nozzle are apparent. The comparatively high contraction ratio (11.5) of the test engine also tends to raise combustion chamber heat flux because of the accompanying low gas velocity near the nozzle entrance, inadequate boundary-layer development, and substantial recirculation. Such high heat flux (relative to the Bartz equation predictions) is frequently observed in high-contraction-ratio combustion chambers.[16] Circumferential variations in combustion chamber heat flux were not significant.

Altitude Performance

Measured Specific Impulse

The simulated altitude firings were carried out with a 60:1 expansion ratio nozzle. A self-starting exhaust diffuser was used to obtain full nozzle flow. Experimental thrust values were obtained in two ways, one directly from load-cell measurements and the other by integration of measured nozzle pressure profiles, with good agreement between the two methods (±1%). Measured, uncorrected, vacuum I_{sp} and I_{sp} efficiency for the five tests which were carried out are shown by the data points and solid curves in Fig. 13. At 25% H_2 and 3.0 F_2/Li mixture ratio, the respective values were 506 lb_f/lb_m/sec and 95%.

Performance losses due to two-phase flow arise mainly from particle/gas thermal and velocity lags. Since these lags develop near the throat and remain nearly constant thereafter, the presence or absence of a condensed phase in the transonic region determines whether two-phase flow losses may be significant. Further, the magnitude of the lags is essentially determined by particle size. Two-phase flow losses are relatively low if the particles are initially small (typically, ≤ 1 μm in diam) and do not grow significantly during the expansion process. Any condensation which occurs downstream of the transonic region has only minor effect on performance.[17] For Li/F_2/H_2 near the stoichiometric F_2/Li mixture ratio, the proportion of condensed material in the combustion chamber and at the throat (Figs. 5 and 6) increases from zero (at 25% H_2 or less) to 30–40% (at 35% H_2). It would therefore be expected that two-phase flow losses would vary accordingly. Since measured I_{sp} efficiencies at 25% and 35% H_2 are equal, it appears that the increased two-phase performance loss accompanying the higher hydrogen percentage is essentially compensated by the lower heat flux loss (Fig. 12). At hydrogen proportions of 20% and 25%, there is no two-phase flow in the throat region; hence the higher heat loss at the lower hydrogen percentage is reflected in correspondingly decreased I_{sp} efficiency.

Analytical calculations of performance losses due to two-phase flow are critically dependent upon the assumed particle sizes of the condensed phase. Since theoretical prediction of particle size is not yet possible and reliable experimental particle size measurements are extremely difficult to make, analytical computations were used to estimate particle sizes from measured performance efficiencies. For Li/F_2/H_2 at the nominal test conditions, calculated[18] condensed phase mass median particle diameters were on the order of 0.5–1.0 μm, reflecting the comparatively low lag losses which were observed.

Deliverable Specific Impulse

Preliminary Li/F_2/H_2 engine system studies now being carried out indicate that regenerative cooling with LH_2 would be feasible for a variety of pump-turbine power cycles appropriate to this tripropellant combination. The measured, uncorrected I_{sp} efficiency and thrust chamber heat flux in each of the altitude simulation tests were therefore used to calculate the I_{sp} deliverable by this type of engine (dashed curves in Fig. 13). Of the five test conditions, the highest vacuum I_{sp} (509 lb_f/lb_m/sec) would occur at 25% H_2 with an F_2/Li mixture ratio of 3.0.

The experimental I_{sp} and heat flux data can be extrapolated to obtain an estimate of the vacuum I_{sp} deliverable by a flight-type, regeneratively cooled, LLi/LF_2/LH_2 engine. At feasible operating conditions (P_c = 1000 psia, F_2/Li MR = 2.74, H_2 = 25%, bell nozzle with ϵ = 100), the estimate is 523 lb_f/lb_m/sec.

Summary and Conclusions

This study has experimentally demonstrated the feasibility of the Li/F_2/H_2 tripropellant combination. The very small Li droplets required for efficient combustion may be produced by aerodynamic atomization of LLi, using the combustion products of an oxidizer-rich or fuel-rich F_2/H_2 gas generator as gas source. Correlations for the development of injector design criteria for this type of atomization were established. Corrected c^* efficiencies of 97–99% were obtained with thrust chamber configurations based on either type of gas generator.

Measured heat flux levels in the nozzle were somewhat below those predicted by the Bartz simplified equation. With water-cooled hardware, the heat transfer characteristics in the combustion chamber and at the entrance region of the convergent nozzle were complicated by the presence of condensed material deposited on the walls. This coating had two opposing, time-dependent effects on heat flux: an enhancement, due to the heat of condensation, and a reduction, due to the thermal barrier formed after deposition. The heat flux measurements showed that regenerative cooling would be feasible.

Altitude simulation tests with a 60:1 expansion ratio nozzle showed that theoretical performance can be approached in experimental firings. Measured, uncorrected I_{sp} efficiencies were near 95%, corresponding to a vacuum I_{sp} of about 523 lb_f/lb_m/sec deliverable by a regeneratively cooled engine at nominal operating conditions (P_c = 1000 psia, F_2/Li MR = 2.74, H_2 = 25%, ϵ = 100).

References

[1] Arbit, H. A. et. al., "Lithium-Fluorine-Hydrogen Propellant Study," CR-72325, Feb. 1968, NASA.

[2] Arbit, H. A., Clapp, S. D., and Nagai, C. K., "Lithium-Fluorine-Hydrogen Propellant Investigation," CR-72695, May 1970, NASA.

[3] Gordon, L. J. and Lee, J. B., "Metals as Fuels in Multicomponent Propellants," *ARS Journal*, Vol. 32, No. 4, April 1962, pp. 600–606.

[4] Levy, J. B. and Copeland, B. K. W., "The Kinetics of the Thermal, Hydrogen-Fluorine Reaction. I. Magnesium Reactor," *Journal of Physical Chemistry*, Vol. 67, No. 10, Oct. 1963, pp. 2156–2159.

[5] Levy, J. B. and Copeland, B. K. W., "The Kinetics of the Hydrogen-Fluorine Reaction. II. The Oxygen-Inhibited Reaction," *Journal of Physical Chemistry*, Vol. 69, No. 2, Feb. 1965, pp. 408–416.

[6] Brokaw, R. S., "A Suggested Mechanism for the Hydrogen-Fluorine Reaction," *Journal of Physical Chemistry*, Vol. 69, No. 7, July 1965, pp. 2488–2489.

[7] Kapralova, G. A., Trofimova, E. M., and Shilov, A. E., "The Upper Ignition Limit in the Reaction of Fluorine with Hydrogen," *Kinetics and Catalysis*, Vol. 6, No. 6, Nov.-Dec. 1965, pp. 884–888.

[8] Semenov, N. N., *Some Problems in Chemical Kinetics and Reactivity*, Vol. I, Princeton University Press, Princeton, N.J., 1958.

[9] Laidler, K. J. and Polanyi, J. C., "Theories of the Kinetics of Bimolecular Reactions," *Progress in Reaction Kinetics*, edited by G. Porter, Vol. 3, Pergamon Press, New York, 1965, pp. 1–61.

[10] Brzustowski, T. A. and Glassman, I., "Spectroscopic Investigation of Metal Combustion," *AIAA Progress in Astronautics and Aeronautics: Heterogeneous Combustion*, edited by H. G. Wolfhard et. al., Vol. 15, Academic Press, New York, 1964, pp. 41–74.

[11] Lambiris, S., Combs, L. P., and Levine, R. S., "Stable Combustion Processes in Liquid Propellant Rocket Engines," *Combustion and Propulsion, Fifth AGARD Colloquium*, Advisory Group for Aeronautical Research and Development, NATO, Macmillan, New York, 1963, pp. 569–636.

[12] Wolfe, H. E. and Andersen, W. H., "Kinetics, Mechanism, and Resultant Droplet Sizes of the Aerodynamic Breakup of Liquid Drops," Rept. 0395-04(18)SP, April 1964, Aerojet-General Corporation, Downey, Calif.

[13] Ingebo, R. D., "Penetration of Drops into High-Velocity Airstreams," TM X-1363, Nov. 1966, NASA.

[14] Rabin, E., Schallenmueller, A. R., and Lawhead, R. B., "Displacement and Shattering of Propellant Droplets," TR 60-75, March 1960, Air Force Office of Scientific Research.

[15] Bartz, D. R., "A Simple Equation for Rapid Estimation of Rocket Nozzle Convective Heat Transfer Coefficients," *Jet Propulsion*, Vol. 27, No. 1, Jan. 1957, pp. 49–51.

[16] Bartz, D. R., "Turbulent Boundary-Layer Heat Transfer from Rapidly Accelerating Flow of Rocket Combustion Gases and of Heated Air," *Advances in Heat Transfer*, edited by J. P. Hartnett and T. F. Irvine, Jr., Vol. 2, Academic Press, New York, 1965, pp. 1–108.

[17] Hoglund, R. F., "Recent Advances in Gas-Particle Nozzle Flows," *ARS Journal*, Vol. 32, No. 5, May 1962, pp. 662–671.

[18] Rannie, W. D., "Perturbation Analysis of One-Dimensional Heterogeneous Flow in Rocket Nozzles," *ARS Progress in Astronautics and Rocketry: Detonation and Two-Phase Flow*, Vol. 6, edited by S. S. Penner and F. A. Williams, Academic Press, New York, 1962, pp. 117–144.